The Interaction of Oxygen with Reduced SnO_2 and Ti/SnO_2 (110) Surfaces: A Density Functional Theory Study

Yoichi Yamaguchi*

Kansai Research Institute, Kyoto Research Park 17, Chudoji Minami-machi, Shimogyo-ku, Kyoto 600-8813, Japan

Yosuke Nagasawa,† Kenji Tabata, and Eiji Suzuki

Research Institute of Innovative Technology for the Earth, 9−2, Kizugawadai, Kizu-cho, Soraku-gun, Kyoto 619-0292, Japan

Received: May 1, 2001; In Final Form: October 18, 2001

Density functional theory calculations within the generalized gradient approximation have been performed for the interaction of oxygen with reduced SnO_2 and Ti/SnO_2 (110) surfaces. We found small dissociation energies for a peroxo species on both surfaces and slightly lower migration barriers of ∼6−13 kcal/mol for an oxygen atom produced by the dissociation of O_2 on the Ti/SnO_2 surface compared to migration barriers of ∼13−18 kcal/mol on the SnO_2 surface. An analysis of the electronic density of states indicates that an adsorbed oxygen atom coupled with the nearest neighboring bridging oxygen vacant site should be an O^- species with catalytic activity on the surfaces. The maximum concentration of O^- species on the perfectly reduced SnO_2 surface is half the concentration of the vacant bridging oxygen sites, which favors yielding a higher concentration of O^- compared to the reduced Ti/SnO_2 surface. The limited migration of the O^- species on the reduced Ti/SnO_2 surface may be an advantage for controlling the catalytic activity. The theoretical reaction rates for the dissociation, recombination, and desorption of adsorbed oxygen species on the surfaces have been discussed using transition-state theory.

I. Introduction

Because of its catalytic importance for the selective oxidation of methane to C_1-oxygenates (methanol and formaldehyde), anionic oxygen species on metal oxides have been an attractive subject of study[1] that is expected to benefit not only the petrochemical industry but also the environment.[2] Although a wide range of metal−oxide catalysts have been reported as active catalysts in reference to this subject, the products are predominantly comprised of CO, CO_2, and H_2O with only traces of C_1−oxygenates. We have also studied this subject using a reduced SnO_2 catalyst[3−8] with the aim of developing a one-step reaction at a lower temperature (∼300−400 K) and pressure (∼1 atm) than those of current commercial processes. However, we have only detected the trace formations of oxygenated intermediates (e.g., methoxy species) and C_1−oxygenates at room temperature by X-ray photoelectron spectroscopy (XPS) measurements.[3,4]

Schematic structures for the thermodynamically most stable SnO_2 (110) surface with the tetragonal rutile lattice are shown in Figure 1. The stoichiometric surface of SnO_2 (110) is formed by 5-fold or 6-fold coordinated Sn^{4+} cations and O^{2-} anions[9] (see Figure 1a). As is well-known, the reduced SnO_2 (110) surface formed by the removal of the top-layer bridging oxygens from the stoichiometric surface is an *n*-type semiconductor, resulting in useful technological applications, e.g., chemical gas-sensing devices[10] using the change in the electrical conductivity due to the surface O/Sn ratio.[11] The removal of a bridging oxygen leaves two electrons, resulting in the reduction of tin from a 6-fold coordinated Sn^{4+} to a 4-fold coordinated Sn^{2+} (see Figure 1b), with which an oxygen molecule can interact.

From ESR measurements, it has been suggested that an adsorbed O_2 molecule is changed to various anionic oxygen species by transfer of an electron from the Fermi level of the reduced SnO_2 in the following manner (g = gas, ad = adsorption, lat = lattice):[12]

$$O_2(g) \rightleftharpoons O_2\,(ad) \underset{-e}{\overset{+e}{\rightleftharpoons}} O_2^-\,(ad) \underset{-e}{\overset{+e}{\rightleftharpoons}} O_2^{2-}\,(ad) \underset{-e}{\overset{+e}{\rightleftharpoons}} O^-(ad)$$
$$O^{2-}\,(ad) \underset{-e}{\overset{+e}{\rightleftharpoons}} O^{2-}\,(lat) \quad (1)$$

The O_2^-, O_2^{2-}, and O^- species on a reduced SnO_2 surface have been experimentally detected,[3,12−14] and it has been confirmed that O^- acts as a highly active catalytic center for hydrogen abstraction from methane on metal−oxide surfaces[15] on the basis of theoretical and experimental results.[5,16−24] We have also theoretically found that the order of the energy barriers for this reaction is O_2^- (48 kcal/mol) >> O^- (12 kcal/mol) on a point-charge model corresponding to the reduced SnO_2 (110) surface,[5] which is a value similar to the previous theoretical results in the range of 6−16 kcal/mol on other metal oxides.[16−18] On the other hand, the measurements indicate no existence of a lower active O_2^- species on a reduced SnO_2 surface.[4] Because of the higher catalytic activity of O^- species on a reduced SnO_2 surface than the O_2^- species on the noble metal surfaces,[25] C_1−oxygenates are successively oxidized by O^- to CO or CO_2 on the former. One then needs to examine whether we can control the reactivity, concentration, and migration of an O^- species in

* To whom correspondence should be addressed.
† Permanent address: Osaka Gas Co., 1-1-3 Hokkou-Shiratsu, Konohana-ku, Osaka 554-0041, Japan.

10.1021/jp011638f CCC: $22.00 © 2002 American Chemical Society
Published on Web 12/06/2001

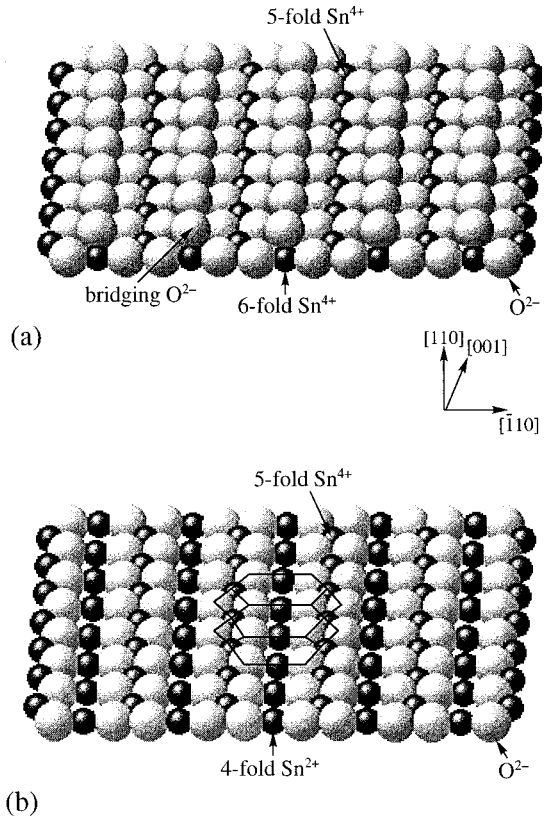

Figure 1. Schematic structures for (a) the stoichiometric and (b) the reduced SnO_2 (110) surfaces. The bold lines shown on the reduced surface represent the area of the model cluster.

order to efficiently yield C_1-oxygenates on the metal−oxide catalysts. With this objective, we examined the influence of the substitution of Ti atoms for the 4-fold coordinated Sn^{2+} of a reduced SnO_2 (110) surface on the scheme of eq 1. TiO_2 is one of the isostructural metal−oxides with SnO_2, which also has a thermally stable (110) surface[26−28] with a closer lattice constant ($a = 4.594$ Å, $c = 2.958$ Å[29]) to that ($a = 4.737$ Å, $c = 3.186$ Å[29]) of SnO_2.

In this study, we present the results of the density functional theory (DFT) calculations for the interaction of oxygen with a reduced Ti/SnO_2 (110) surface and compared with the calculated results on a reduced SnO_2 (110) surface.

II. Method of Calculation

All of the present DFT calculations were carried out using the DMol[3] program package provided by Molecular Simulations Inc. (MSI).[30] All electrons were treated in the geometrical optimization for the adsorbed oxygen species on the monolayer reduced Ti/SnO_2 (110) cluster within the generalized gradient approximation (GGA), including the relativistic effects level of theory using the Becke-Lee−Yang−Parr nonlocal type functional (BLYP). The geometries of all the present clusters were fixed at an SnO_2 crystal.[29,31] The vibrational frequencies of the adsorbed O_2 molecule and the transition state for its dissociation on the monolayer clusters were also calculated using the same level of theory in order to estimate the first-order rate constants of the dissociation, recombination, and desorption of oxygen species at 1 atm using transition-state theory. Also on the basis of the optimal structures, single-point GGA energies for the three-layer reduced Ti/SnO_2 (110) clusters with oxygen were calculated using the effective core potential (ECP) and BLYP levels of theory. A Fermi surface thermal smearing parameter of 0.02 atomic units was used in order to be arrived at self-consistent field (SCF) convergence of the present calculations. The basis sets used throughout were the standard double numerical atomic basis sets plus *d*-functions (DND). The Madelung potential is not applied to the present calculations, though we have checked that the Coulomb interaction from the outside of the cluster is significantly weakened by the screening effect. Although it is important to consider the surface relaxation during the adsorption of oxygen to the reduced surface, it needs the geometrical optimization of a surface model with a large number of heavy Sn atoms using the band theory calculations that demands the extreme computational cost. We therefore did not consider the surface relaxation in this study.

The topmost layer of a reduced SnO_2 (110) cluster is indicated by the bold lines in Figure 1b. Figure 2 shows the schematic stoichiometric and reduced three-layer SnO_2 clusters that are respectively clipped out from the surfaces in Figure 1a,b. The present three-layer cluster is a fully reduced structure formed by the removal of bridging oxygens on both sides of the cluster in order to make a clear distinction between the electronic structures of the reduced and the stoichiometric clusters. The corresponding monolayer clusters are formed by the top-layer containing the inner three bridging oxygen atoms in each three-layer cluster. In Figure 2, the substituted four (two) Ti atoms for Sn atoms exist in the symmetrical equivalent site B in both the stoichiometric and reduced three (mono)-layer cluster. The monolayer and three-layer reduced (stoichiometric) Ti/SnO_2 clusters are, respectively, $Sn_8Ti_2O_{15}$ ($Sn_8Ti_2O_{18}$) with C_{2v} symmetry and $Sn_{27}Ti_4O_{50}$ ($Sn_{27}Ti_4O_{56}$) with D_{2h} symmetry. All of the present clusters are electrically neutral species. Although there is a lack of information on the adsorption sites of the O_2 molecule on a reduced Ti/SnO_2 and SnO_2 (110) surface, we assume that it adsorbs at a vacant bridging oxygen site on each surface, as on the TiO_2 (110) surface.[32] We doubt the validity of the distribution of the spin densities of the cluster with the open-shell oxygen species because the present DFT level of the unrestricted GGA calculations indicates that the spin densities exist predominantly in the reduced clusters, not in the adsorbed O_2^- species. Therefore, we set the singlet spin state for all the present clusters with oxygen. Similar DFT calculations have been conducted for the interaction of oxygen with the SnO_2 (110) surfaces for comparison. A Silicon Graphics Origin 2000 R10000 workstation was used for the present calculations.

III. Results and Discussion

A. Substitution sites of Ti. To our knowledge, the substitution site of Ti for Sn on a SnO_2 crystal with the rutile structure is not known. We therefore examined theoretically the energetic stability of alternative substitution sites for a Ti atom replacing a Sn atom on the surface using the three-layer stoichiometric $Sn_{30}TiO_{56}$ and reduced $Sn_{30}TiO_{50}$ clusters. The results of the single-point calculations at the GGA level for these clusters are summarized in Table 1; here the substitution sites are defined in Figure 2. The energy of the 6-fold coordinated Ti^{4+} at site A of each cluster is taken as a reference. We found that the stoichiometric and reduced Ti/SnO_2 surfaces provide the most stable structures when there is a substitution of a Ti atom for the 6-fold coordinated Sn^{4+} at sites B and A, respectively. The relative stability of the 5-fold coordinated Ti^{4+} at site C does not change between the stoichiometric and reduced clusters, indicating a small influence by the abstraction of the bridging oxygens on Ti at site C, which is supported by the small change in the net charges in Table 1. There is a smaller change in the net charge in Ti at site A between the stoichiometric and reduced

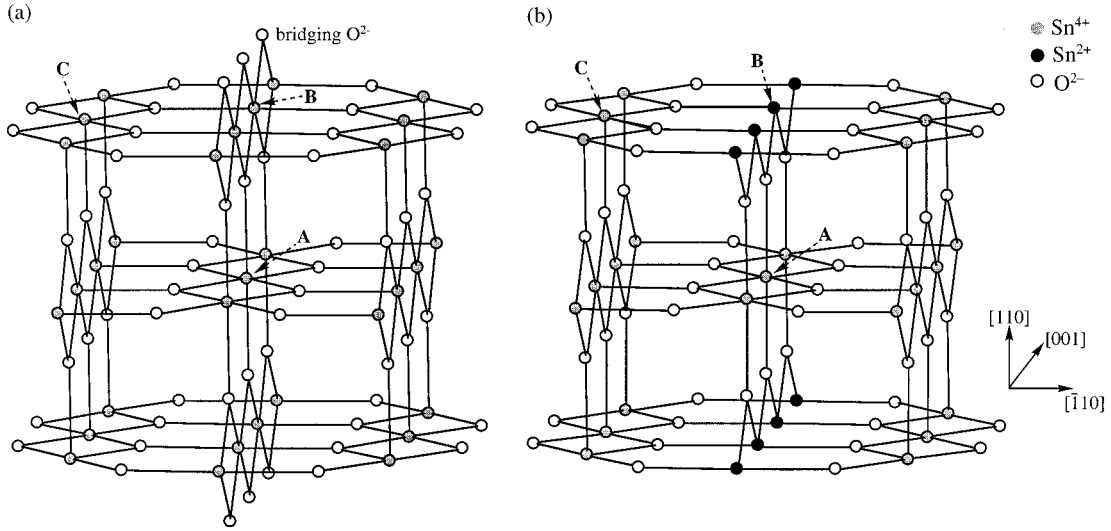

Figure 2. Schematic three-layer structures for (a) the stoichiometric and (b) the reduced SnO_2 (110) clusters. The substitution sites A, B, and C of a Ti atom for a Sn atom on the models are shown.

TABLE 1: Relative Energies RE (kcal/mol) and Mulliken Atomic Net Charges (|e|) at Each Substitute Site[a] of a Ti Atom for a Sn Atom in the Three-Layer Stoichiometric and Reduced SnO_2 Clusters

		stoichiometric cluster		reduced cluster	
atom	site	RE	net charge	RE	net charge
Ti (Sn)	A	0.0	+1.42 (+1.90)	0.0	+1.39 (+1.89)
	B	−1.8	+1.35 (+1.78)	22.6	+1.00 (+1.19)
	C	6.4	+1.28 (+1.54)	6.5	+1.22 (+1.47)

[a] Defined in Figure 2. Values in parentheses are for the Sn atom at each site before substitution.

Ti/SnO_2 clusters even compared to the Ti at site C. On the other hand, it is natural to note that the electron-rich 4-fold coordinated Ti^{2+} at site B in a reduced surface has the ability to interact with an oxygen molecule, such as a Sn^{2+} at the same site in the reduced SnO_2 surface, due to the decreased positive net charge, namely, increased electron density at that site after the reduction.

It should be noted that because the metal−oxide catalysts are conventionally prepared under oxidative conditions in order to yield less oxygen defects, we can only obtain a stoichiometric Ti/SnO_2 catalyst with the 6-fold coordinated Ti^{4+} at site B. For a stoichiometric SnO_2 (110) surface, the topmost bridging oxygens on the surface can be easily removed by heating at >700 K in a vacuum[11] or by a particle bombardment process.[33] On the other hand, for a stoichiometric TiO_2 with the rutile structure, it seems difficult to produce a reduced surface due to a significantly stronger $Ti^{4+}-O-Ti^{4+}$ bridging bond. However, for a stoichiometric Ti/SnO_2 surface, we think that the random substitution of Ti for Sn at site B occurs, which produces the predominant formation of a $Sn^{4+}-O-Sn^{4+}$ bridging bond and a $Ti^{4+}-O-Sn^{4+}$ bridging bond rather than a $Ti^{4+}-O-Ti^{4+}$ bridging bond for a low concentration of Ti. Thus, we expect that a bridging oxygen in the former should be easier to remove by the above experimental processes than that in the latter on the Ti/SnO_2 surface. Because of the extreme cost of the present DFT calculations for the Ti/SnO_2 clusters with the asymmetrical Ti−O−Sn structure in the center of the surface, we used the simplified Ti/SnO_2 clusters with the symmetrical Ti−O−Ti structure in the center of the surface, as shown in Figure 4. Therefore, the calculated results using the present SnO_2 and Ti/SnO_2 clusters will approximately provide upper and lower limits of data (e.g., adsorption energies) in comparison with the measurements on a prepared Ti/SnO_2 catalyst under the conditions of various concentrations of Ti.

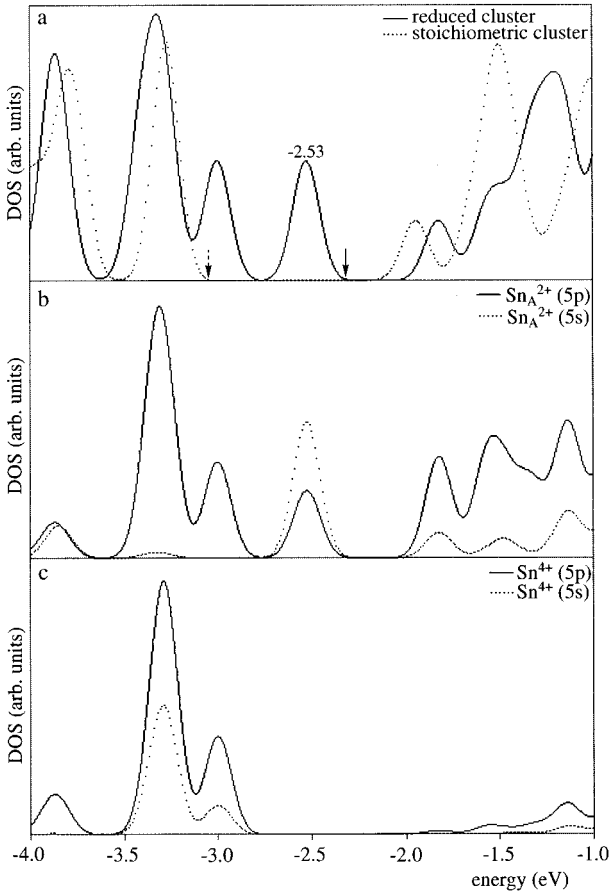

Figure 3. (a) TDOS for the stoichiometric and reduced SnO_2 clusters, (b) PDOS for 4-fold Sn_A^{2+}, and (c) PDOS for 5-fold Sn^{4+}, of the reduced SnO_2 cluster. The arrows mark the energies of the highest occupied states, namely, the Fermi energy. The positions of 4-fold Sn_A^{2+} and 5-fold Sn^{4+} are defined in Figure 4.

B. Interaction of Oxygen with SnO_2 Surface. First, we will discuss the calculated results of the interaction of oxygen with the reduced SnO_2 cluster, which is useful for understanding the interaction of oxygen with the reduced Ti/SnO_2 cluster. Figure 3a shows the total electronic densities of state (TDOS) near the Fermi level of the three-layer stoichiometric and reduced SnO_2

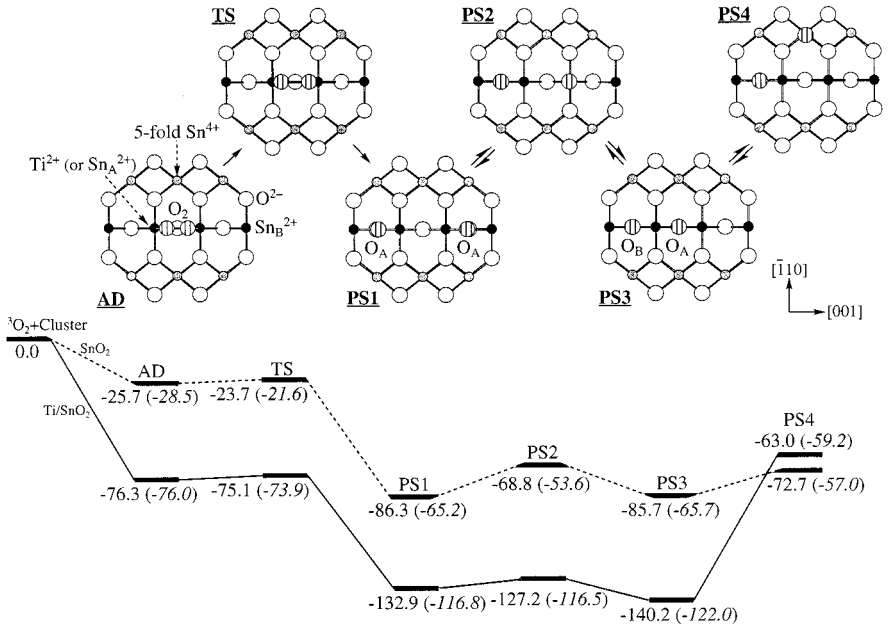

Figure 4. Potential energy diagram for adsorption (AD), dissociation (TS), and migration (PS1−PS4) of oxygen on the three-layer reduced SnO_2 and Ti/SnO_2 clusters. The parentheses represent the values of each monolayer reduced cluster. Relative energies are given in kcal/mol. The top of view of the clusters with the adsorbed oxygen species.

TABLE 2: Calculated Results for the Adsorbed O_2 Molecules on the Mono and Three-Layer Reduced Ti/SnO_2 and SnO_2 (110) Clusters

		Ti/SnO_2 (110)			SnO_2 (110)		
	end-on	side-on	TS[e]	end-on	end-on	side-on	TS[e]
bond lengths (Å)[a]	O−O	1.383	1.449	1.652	1.347	1.435	1.909
	Ti^{2+} (or Sn_A^{2+})[c]−O	2.113	1.994	1.908	2.386	2.226	2.066
vibrational frequencies (cm^{-1})[a]	ν(O−O)	894	705	601i	968	718	661i
adsorption energies (kcal/mol)[b]		63.2	76.3	75.1	16.5	25.7	23.7
Mulliken atomic net charges (|e|)[b]	O_2[d]	−0.63	−0.66	−0.76	−0.58	−0.66	−0.92
	Ti^{2+} (or Sn_A^{2+})[c]	+1.16	+1.16	+1.18	+1.43	+1.47	+1.51

[a] Monolayer model. [b] Three-layer model. [c] The positions are defined in Figure 4. [d] Per molecule. [e] Transition state for the dissociation of the side-on type adsorbed O_2 molecule.

clusters. The reduced cluster has a smaller energy gap (0.36 eV) than that for the stoichiometric cluster 0.98 eV; here the experimental value of a stoichiometric crystal is 3.6 eV.[34] We found that the energy of the highest occupied state of the reduced cluster is pushed up with a new peak at −2.53 eV, which corresponds to extending up to the Fermi level of a reduced SnO_2 (110) surface compared to that of a stoichiometric surface based on the measurements.[35,36] The comparison of the partial electronic densities of state (PDOS) for the 4-fold coordinated Sn_A^{2+} and 5-fold coordinated Sn^{4+} in the three-layer reduced cluster in panels b and c, respectively, of Figure 3 shows that the new peak at −2.53 eV is composed of Sn_A^{2+} (5s and 5p) not Sn^{4+}; here the positions of the selected Sn_A^{2+} and Sn^{4+} are defined in Figure 4. The TDOSs and PDOSs for the three-layer clusters were used in all of the present figures. It can be seen in Table 1 that the decrease in the net positive charge at the Sn_A^{2+} site from the stoichiometric cluster of +1.78 to the reduced cluster of +1.19 with the removal of the bridging oxygens indicates an increased electron density at this site in the reduced cluster, which corresponds to the reduction of tin from a 6-fold coordinated Sn^{4+} to a 4-fold coordinated Sn^{2+}. On the other hand, there is a trivial change in the net charge at the 5-fold coordinated Sn^{4+} site and the inner 6-fold coordinated Sn^{4+} at site A (see also Figure 2). Therefore, we find that the reduction effect is only appeared at the Sn_A^{2+} site in the topmost SnO_2 layer.

The calculated results for the two types of O_2 molecule adsorptions are summarized in Table 2; the side-on type in which O_2 lies flat on the surface and the end-on type where O_2 stands straight on the surface. The net charge of the O_2 molecule attributed to the charge transfer from Sn^{2+} (5s) of the surface to the unoccupied $2p\pi^*$ orbital of the O_2 molecule is somewhat larger in the case of side-on type adsorption (−0.66) than in the end-on type adsorption (−0.58). A larger adsorption energy for the side-on type compared to the end-on type on the three-layer reduced cluster is in agreement with the experimental results.[13] The peroxo (O_2^{2-}) and superoxo (O_2^-) species of the adsorbed O_2 molecule on the metal surfaces have been experimentally observed; the former has an O−O bond length of 1.47 ± 0.05 Å and a vibrational frequency of 645 cm^{-1} on Ag (110), and the latter has an O−O bond length of 1.32 ± 0.05 Å and a vibrational frequency of 887 cm^{-1} on Pt (111).[37] As compared the calculated results in Table 2 with above experimental data, we find that the adsorbed O_2 molecules at the side-on type and the end-on type on the reduced SnO_2 surface are close to a peroxo and a superoxo species, respectively.

The potential energy diagram of the adsorption, dissociation and migration of oxygen on the reduced surface is illustrated in Figure 4. The total energies of the separated $^3O_2$ molecule and the three-layer reduced SnO_2 cluster are taken as a reference. The values for the monolayer reduced cluster are also shown

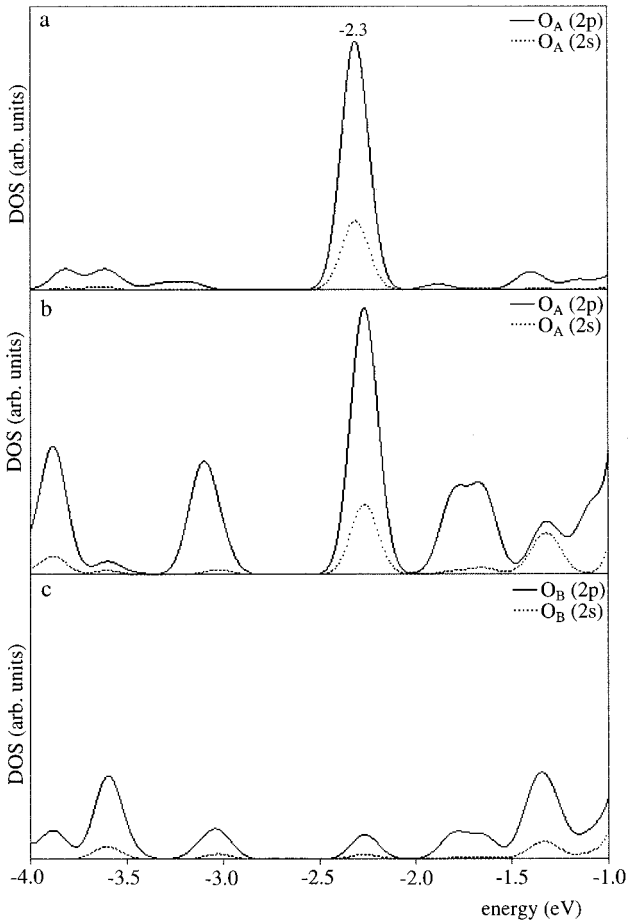

Figure 5. (a) PDOS for O_A of PS1, (b) PDOS for O_A of PS3, and (c) PDOS for O_B of PS3, in the reduced SnO_2 cluster. The oxygen atoms, O_A and O_B, are defined in Figure 4.

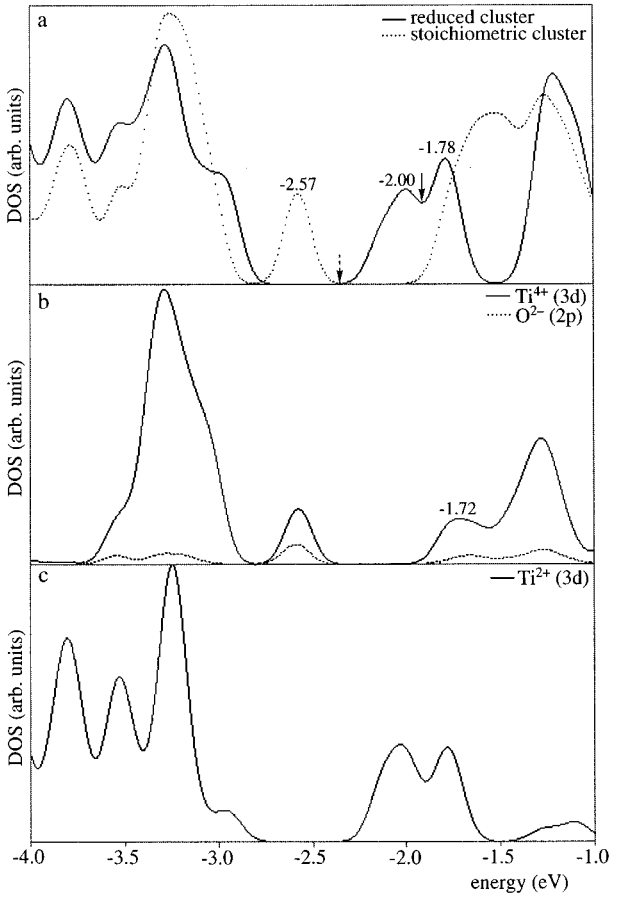

Figure 6. (a) TDOS for the stoichiometric and reduced Ti/SnO_2 clusters, (b) PDOS for 6-fold Ti^{4+} and O^{2-} of the stoichiometric cluster, and (c) PDOS for 4-fold Ti^{2+} of the reduced cluster. The arrows mark the energies of the highest occupied states. The position of 6-fold Ti^{4+} in the stoichiometric surface is one-to-one correspondence to that of 4-fold Ti^{2+} defined in Figure 4.

in parentheses for comparison. The top of view of the clusters with the adsorbed oxygen species is also shown as inserts in Figure 4. We find a small dissociation energy of 2.0 kcal/mol for the O_2 molecule on the three-layer reduced cluster. The transition state (TS) has a shorter Sn_A^{2+}−O bond length and a larger net charge than those of the two types of adsorbed O_2 molecules (see Table 2), indicating the strong interaction of TS with the SnO_2 surface. Next, we explain the migration of an oxygen atom in PS1−PS4. In both the monolayer and three-layer clusters, the net charges of the oxygen atom increase from that at the TS of −0.46 to PS1−PS4 of −0.71 at the bridge oxygen vacant site, indicating that the topmost layer of a reduced SnO_2 surface contributes to the charge transfer from the SnO_2 surface to oxygen. The oxygen atom is stabilized at the vacant bridging oxygen site in PS1 and PS3 and destabilized above the Sn_A^{2+} site in PS2 and above the Sn^{4+} site in PS4. The migration barriers of the oxygen atom on the three-layer cluster between PS1 and PS3 are 16.9−17.5 kcal/mol. The energy difference of 13.0 kcal/mol between PS3 and PS4 corresponds to the migration barrier of the oxygen atom to the nearest neighboring row of Sn^{2+}.

The PDOS for the adsorbed oxygen species of PS1 and PS3 are shown in Figure 5. It can be seen in Figure 5a,b that the PDOS for O_A of PS1 and PDOS for O_A of PS3 have the same strong peaks at −2.3 eV. On the other hand, in Figure 5c, the intensity of this peak in PDOS for O_B of PS3 is significantly weaker; here the DOS in panels b and c of Figure 5 are on the same scale. The absence of a peak at −2.3 eV in the stoichiometric cluster apparent from Figure 3a means that the electronic states of O_A in both PS1 and PS3 are quite different from those of the bridging oxygens on the stoichiometric SnO_2 cluster. Thus, we assume that the O_A coupled with the nearest-neighboring vacant bridging oxygen site in PS1 and PS3 is an O^- (ad) species (see eq 1) with catalytic activity for hydrogen abstraction from methane; here, as mentioned in the methodology, we could not reproduce the spin density of an open-shell O^- species on the reduced SnO_2 surface because the singlet spin state is applied for the present DFT calculations. On the other hand, the O_B uncoupled from this vacant site in PS3 is an O^{2-} (ad) species or an O^{2-} (lat)-like species (see eq 1) with less catalytic activity due to their singlet electronic states.

C. Interaction of Oxygen with Ti/SnO_2 Surface. Next we discuss the calculated results of the interaction of oxygen with the reduced Ti/SnO_2 cluster. The TDOS near the Fermi level of the three-layer stoichiometric and reduced Ti/SnO_2 clusters is shown in Figure 6a, which has slightly complicated structures compared to the above-mentioned SnO_2 clusters. The reduced and stoichiometric clusters show considerably smaller energy gaps of 0 and 0.37 eV, respectively, than those of the corresponding SnO_2 clusters. The TDOS of the stoichiometric cluster has a new peak at −2.57 eV whose position stands in the energy gap of stoichiometric SnO_2 cluster and is composed of Ti^{4+} (3d) and bridging oxygen (2p) (see Figure 6b). The shallower energy level of this Ti^{4+}−O^{2-} bonding orbital in the stoichiometric Ti/SnO_2 cluster indicates a characteristic of an opt-active TiO_2 catalyst. For the reduced cluster, the peak at −2.57 eV is absent, and new peaks appear at −1.78 and −2.00

eV, as shown in Figure 6a. The former is comprised of the vacant orbital of Ti^{2+} (3d), which corresponds to the peak at -1.72 eV of Ti^{4+} (3d) of the stoichiometric cluster. The latter is comprised of the occupied orbital of Ti^{2+} (3d). The Fermi level of the reduced Ti/SnO_2 cluster then stands intermediate between the two new peaks.

From the change in the net positive charge at site B before and after the reduction in Table 1, the increase in the electron density at the Ti^{2+} site in the reduced Ti/SnO_2 cluster is about half of that at the Sn_A^{2+} site in the reduced SnO_2 cluster, indicating the delocalized and localized characteristics for the former and the latter, respectively. Although there are significant greater adsorption energies on the reduced Ti/SnO_2 cluster compared to those on the reduced SnO_2 cluster, the adsorbed O_2 molecules at the side-on type and the end-on type on the former cluster are close to a peroxo and a superoxo species, respectively, such as the case of the latter (see Table 2).

The potential energy diagram of the adsorption, dissociation (TS), and migration of oxygen on the reduced Ti/SnO_2 surface is also shown in Figure 4. There is a small dissociation energy of 1.2 kcal/mol for the O_2 molecule on the three-layer reduced cluster, as for the above-mentioned SnO_2 cluster. In both the monolayer and three-layer clusters, the net charges of the oxygen atom increase from that at the TS of -0.38 to PS1−PS4 of -0.57 at the vacant bridging oxygen site, indicating that the topmost layer contributes to the charge transfer from the Ti/SnO_2 surface to oxygen. The migration barriers of the oxygen atom on the three-layer cluster between PS1 and PS3 are 5.7−13.0 kcal/mol. We think that the energy difference of 77.2 kcal/mol between PS3 of a stationary point and PS4 of a nonstationary point does not represent the migration barrier of the oxygen atom to the nearest neighboring row of Ti^{2+}/Sn^{2+}. We can find that the migration of an oxygen atom from PS3 to PS4 creates a significantly unstable bare 4-fold coordinated Ti^{2+}, as seen in Table 1. Indeed, there is no position, except PS4, with a bare 4-fold coordinated Ti^{2+} in Figure 4. Thus, it is unlikely that an adsorbed oxygen atom can migrate with the formation of a significantly unstable bare 4-fold coordinated Ti^{2+} on the reduced Ti/SnO_2 surface, which is in contrast to demand a small potential energy for creating a bare 4-fold coordinated Sn_A^{2+} on the reduced SnO_2 surface.

The PDOS for the adsorbed oxygen species of PS1 and PS3 are shown in Figure 7. In Figure 7a, the two peaks at -2.17 and -2.42 eV in the PDOS for O_A of PS1 originate, respectively, from a $Ti^{2+}\cdots O_A$ interaction and a $Sn_B^{2+}\cdots O_A$ interaction. The former is assigned using the peak at -2.17 eV in the PDOS for O_A of PS3 in Figure 7b, which has a weaker $Sn_B^{2+}\cdots O_A$ interaction. No peak separation in the PDOS for O_A of PS1 in the reduced SnO_2 cluster (see Figure 5a) indicates a small difference in the electronic states between Sn_A^{2+} and Sn_B^{2+}. Due to the absence of the peak at -2.17 eV in the stoichiometric Ti/SnO_2 cluster, the electronic states of O_A in both PS1 and PS3 are different from those of the bridging oxygens. Thus, O_A coupled with the nearest-neighboring vacant bridging oxygen site in PS1 and PS3 should also be an O^- (ad) species (see eq 1) with catalytic activity, similar to O_A on the reduced SnO_2 cluster. However, we cannot predict the difference in the catalytic activity between O_A on the reduced Ti/SnO_2 and SnO_2 surfaces. On the other hand, for O_B of PS3 in Figure 7c, there are two peaks at -2.51 and -2.71 eV in its PDOS, whose separation originates from the asymmetrical interaction, as also seen in O_A of PS1; here the PDOS in panels b and c of Figure 7 are on the same scale. Apparently, it seems that O_B of PS3 is also the catalytically active O^- species, like O_A of PS1 and

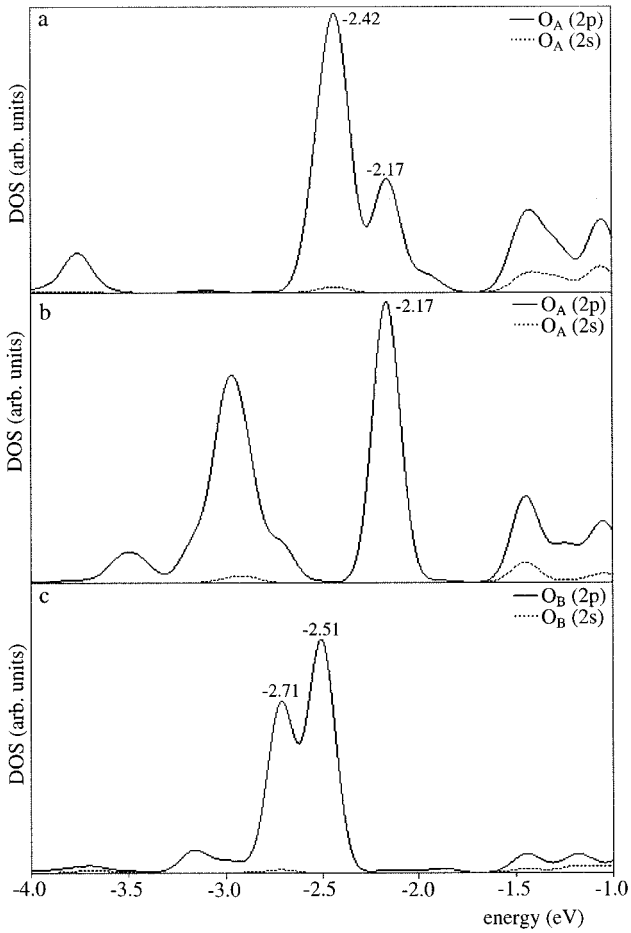

Figure 7. (a) PDOS for O_A of PS1, (b) PDOS for O_A of PS3, and (c) PDOS for O_B of PS3, in the reduced Ti/SnO_2 cluster. The oxygen atoms, O_A and O_B, are defined in Figure 4.

PS3, because there is no corresponding peak with a considerable intensity in the PDOS for O_B of the reduced SnO_2 cluster. However, we think that the above two peaks for O_B of PS3 originate in the peak at -2.57 eV of a Ti−O bonding orbital in the stoichiometric Ti/SnO_2 cluster. Thus, we think that the O_B uncoupled from the bridging oxygen vacant site in PS3 should be an O^{2-} (ad) species or an O^{2-} (lat)-like species (see eq 1) without catalytic activity, like O_B on the reduced SnO_2 cluster.

Finally, we estimated the first-order rate constants of three elemental reactions; the dissociation of AD → TS, the recombination of PS1 → TS, and the desorption of AD → ($^3O_2$ + Cluster) on the monolayer SnO_2 and Ti/SnO_2 surfaces using transition-state theory. Here the notations are in Figure 4. We treated the desorption of an O_2 molecule from a reduced model as a pseudo first-order reaction in order to compare it to the other rate constants. The calculated rate constants of these reactions versus temperature are plotted in Figure 8. It is natural that there are larger rate constants for the dissociation compared to the desorption and recombination because of the small dissociation energies of an adsorbed O_2 molecule in both the SnO_2 and Ti/SnO_2 surfaces. However, there are significant increases in the rate constants for the desorption and recombination with increasing temperature in contrast to those of the dissociation. Although the rate-determining step for the abstraction of O_2 from a reduced SnO_2 surface is the recombination of adsorbed oxygen atoms, we find that the rate constant of the desorption is nearly eqaul to that of the dissociation at >700−800 K due to the advantage of entropy for the desorption, which represents the experimental abstraction of O_2 from the surface

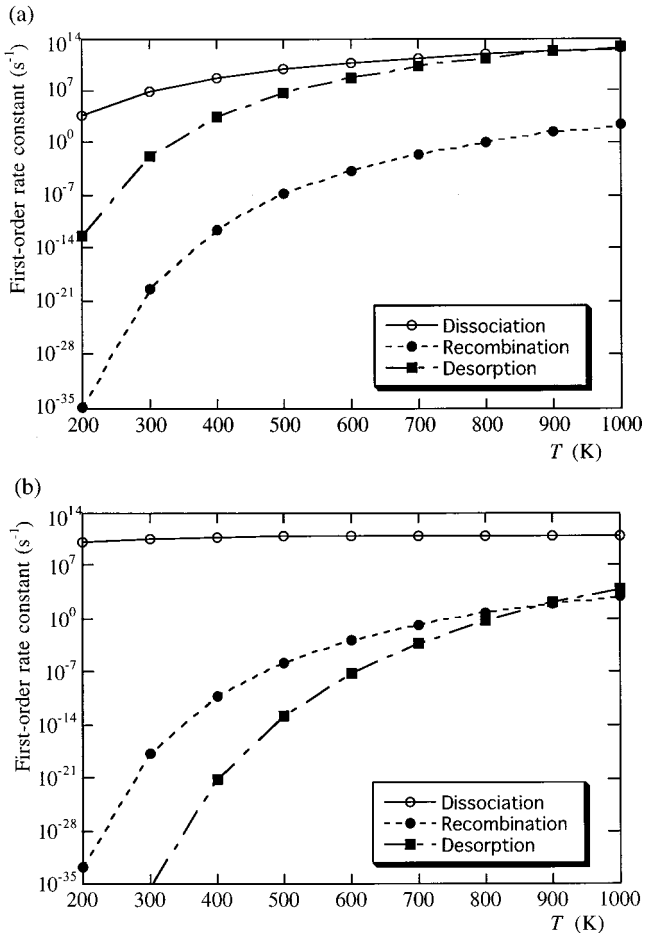

Figure 8. Calculated first-order rate constants for the dissociation, recombination, and desorption of the adsorbed oxygen species on the monolayer reduced (a) SnO_2 and (b) Ti/SnO_2 clusters.

by a heating process >700 K.[11] On the other hand, for a reduced Ti/SnO_2 surface, an adsorbed O_2 molecule can hardly desorb from the surface at ~1000 K due to its higher barrier of about 76 kcal/mol compared to a reduced SnO_2 surface.

As already mentioned, the other adsorbable site of an O_2 molecule is an inserted vacant bridging oxygen site in the $Ti^{2+}\cdot\cdot\cdot Sn^{2+}$ structure when there is a low concentration of Ti on a reduced Ti/SnO_2 surface. Considering the data in Figure 8, it is unlikely to desorb an O_2 molecule at the $Ti^{2+}\cdots O_2\cdots Sn^{2+}$ site by a heating process <1000 K. Thus by heating at <1000 K we can only remove an O_2 molecule at the $Sn^{2+}\cdots O_2\cdots Sn^{2+}$ site on a reduced Ti/SnO_2 surface. Therefore, because the bridging oxygens connected to Ti will remain on the Ti/SnO_2 surface even after the reduction, which disturbs the adsorption of O_2 in the gas phase, the number of adsorbable O_2 molecules to the surface should be limited. After dissociation of an O_2 molecule on a reduced Ti/SnO_2 surface, an adsorbed oxygen atom can hardly migrate with the formation of a significantly unstabler bare 4-fold coordinated Ti^{2+}, which is in contrast to lower limited migration of an adsorbed oxygen atom on the reduced SnO_2 surface.

Therefore, we theoretically indicated that the present reduced surfaces have the ability to form a highly catalytic active O^- for hydrogen abstraction from methane, which supports the recent experimental data[8] and is different from the noble metal surfaces[25] that can only form a lower active O_2^-. For the reduced SnO_2 (110) surface, we expect that the maximum concentration of the catalytically active O^- species is half the concentration of the vacant bridging oxygen sites, which is an advantage for yielding a higher concentration of O^- species compared to a reduced Ti/SnO_2 surface. However, a lower limited migration of O^- on the former will accelerate the further oxidation of C_1-oxygenates to CO or CO_2. On the other hand, for the reduced Ti/SnO_2 (110) surface, it may be expected that the limited adsorption of an O_2 molecule and limited migration of O^- favor the selective oxidation of methane.

IV. Conclusions

A theoretical study of the interaction of oxygen with reduced SnO_2 and Ti/SnO_2 (110) surfaces has been performed employing DFT within the GGA. We found two species of chemisorbed O_2 molecules that can be described as a peroxo species, O_2^{2-} for side-on type adsorption and a superoxo species and O_2^- for end-on type adsorption in both surfaces. There are small dissociation energies of chemisorbed O_2 molecules as a peroxo species at the bridging oxygen vacant site on both surfaces and a slightly lower migration barrier of oxygen atoms on the reduced Ti/SnO_2 surface compared to that on the reduced SnO_2 surface. The adsorbed oxygen atom coupled with the nearest neighboring bridging oxygen vacant site should be a catalytically active O^- species on the surfaces. The maximum concentration of O^- species on the perfectly reduced SnO_2 surface is half the concentration of the vacant bridging oxygen sites, which will be an advantage for producing a higher concentration of O^- compared to the reduced Ti/SnO_2 surface. However, the further oxidation of C_1-oxygenates to CO or CO_2 will occur due to the lower limited migration of O^- on the SnO_2 surface. On the other hand, for the reduced Ti/SnO_2 surface, the limited adsorption of an O_2 molecule and limited migration of the O^- species may favor the selective oxidation of methane as expected. We also found theoretically that the desorption of a peroxo species on the reduced SnO_2 surface occurs at >700−800 K, which well represents the experimental data.

Acknowledgment. This work was partially supported by the New Energy and Industrial Technology Development Organization (NEDO), Environmental Catalyst Research Project.

References and Notes

(1) See, for instance: Krylov, O. V. *Catal. Today* **1993**, *18*, 209 and references therein.
(2) Firor, F. *The Changing Atmosphere*; Yale University Press: New Haven, CT, 1990; p 52.
(3) Nagasawa, Y.; Choso, T.; Karasuda, T.; Shimomura, S.; Ouyang, F.; Tabata, K.; Yamaguchi, Y. *Surf. Sci.* **1999**, *433*−*435*, 226.
(4) Kawabe, T.; Shimomura, S.; Karasuda, T.; Tabata, K.; Suzuki, E.; Yamaguchi, Y. *Surf. Sci.* **2000**, *448*, 101.
(5) Yamaguchi, Y.; Nagasawa, Y.; Murakami, A.; Tabata, K. *Int. J. Quantum Chem.* **1998**, *69* 669.
(6) Yamaguchi, Y.; Nagasawa, Y.; Shimomura, S.; Tabata, K. *Int. J. Quantum Chem.* **1999**, *74* 423.
(7) Yamaguchi, Y.; Nagasawa, Y.; Shimomura, S.; Tabata, K.; Suzuki, E. *Chem. Phys. Lett.* **2000**, *316*, 477.
(8) Kawabe, T.; Tabata, K.; Suzuki, E.; Yamaguchi, Y.; Nagasawa, Y. *J. Phys. Chem. A* **2001**, *105*, 4239.
(9) Cox, P. A.; Egdell, R. G.; Harding, C.; Patterson, W. R.; Tavener, P. J. *Surf. Sci.* **1982**, *123*, 179.
(10) See for instance, Madou, M. J.; Morrison, S. R. *Chemical Sensing With Solid State Devices*; Academic: Boston, MA, 1989.
(11) Cox, D. F.; Fryberger, T. B.; Semancik, S. *Phys. Rev. B* **1988**, *38*, 2072.
(12) Mizokawa, Y.; Nakamura, S. *Ohyo Buturi* **1977**, *46*, 580.
(13) Meriaudeau, P.; Naccache, C.; Tench, A. J. *J. Catal.* **1971**, *21*, 208.
(14) Shen, G. L.; Casanova, R.; Thornton, G. *Vacuum* **1992**, *43*, 1129.
(15) See for instance, Mehandru, S. P.; Anderson, A. B.; Brazdil, J. F. *J. Am. Chem. Soc.* **1988**, *110*, 1715.
(16) Mehandru, S. P.; Anderson, A. B.; Brazdil, J. F.; Grasselli, R. K. *J. Phys. Chem.* **1987**, *91*, 2930.
(17) Bfrve, K. J.; M. Pettersson, L. G. M. *J. Phys. Chem.* **1991**, *95*, 7401.

(18) Bfrve, K. J. *J. Chem. Phys.* **1991**, *95*, 4626.
(19) Goto, A.; Aika, K. *Bull. Chem. Soc. Jpn.* **1998**, *71*, 95.
(20) Driscoll, D. J.; Martir, W.; Wang J. X.; Lunsford, J. H. *J. Am. Chem. Soc.* **1985**, *107*, 58.
(21) Au, C. T.; Roberts, M. W. *J. Chem. Soc., Faraday Trans. I* **1987**, *83*, 2047.
(22) Hutchings, G. J.; Scurrell, M. S.; Woodhouse, J. R. *J. Chem. Soc., Chem. Commun.* **1987**, 1388.
(23) Anpo, M.; Sunamoto, M.; Doi, T.; Matsuura, I. *Chem. Lett.* **1988**, 701.
(24) Cant, N. W.; Lukey, C. A.; Nelson, P. F.; Tyler, R. J. *J. Chem. Soc., Chem. Commun.* **1988**, 766.
(25) Nakatsuji, H.; Hu, Z.-M.; Nakai, H.; Ikeda, K. *Surf. Sci.* **1997**, *387*, 328.
(26) Ramamoorthy, M.; Vanderbilt, D.; King-Smith, R. D. *Phys. Rev. B* **1994**, *49*, 16721.
(27) Charlton, G.; Howes, P. B.; Nicklin, C. L.; Steadman, P.; Taylor, J. S. G.; Muryn, C. A.; Harte, S. P.; Mercer, J.; McGrath, R.; Norman, D.; Turner, T. S.; Thornton, G. *Phys. Rev. Lett.* **1997**, *78*, 495.
(28) Oviedo, J.; Gillan, M. J. *Surf. Sci*. **2000**, *463*, 93.
(29) Wyckoff, R. *Crystal Structures*, 2nd ed.; Wiley: Interscience: New York, 1964; Vol. 1.
(30) Delley, B. *J. Chem. Phys.* **1990**, *92*, 503. DMol^3, ver. 4.2, of the Cerius^2 program suite is available from Molecular Simulations Inc., San Diego, CA.
(31) See for instance, Henrich, V. E.; Cox, P. A. *The Surface Science of Metal Oxides*; Cambridge University Press: Cambridge, 1994; p 43.
(32) Gopel, W. *Prog. Surf. Sci.* **1985**, *20*, 9.
(33) de Frësart, E.; Darville, J.; Gilles, J. M. *Appl. Surf. Sci.* **1982**, *11/12*, 637.
(34) Agekyan, V. T. *Phys. Status Solidi A* **1975**, *43*, 11.
(35) Egdell, R. G.; Ericksen, S.; Flavell, W. R. *Solid State Commun.* **1986**, *60*, 835.
(36) Cox, D. F.; Fryberger, T. B.; Erickson, J. W.; Semancik, S. *J. Vac. Sci. Technol., A* **1987**, *5*, 1170.
(37) Outka, D. A.; Stoehr, J.; Jark, W.; Stevens, P.; Solomon, J.; Madix, R. J. *Phys. Rev. B* **1987**, *35*, 4119.